Reaction Pathways of Iron Trifluoride Investigated by Operation at 363 K Using an Ionic Liquid Electrolyte

Shinya Tawa, Kazuhiko Matsumoto, *,z and Rika Hagiwara *

Graduate School of Energy Science, Kyoto University, Yoshida-honmachi, Sakyo-ku, Kyoto 606-8501, Japan

FeF_3 possesses a high theoretical capacity of 712 mAh g^{-1} owing to the three-electron reaction. However, various drawbacks, such as the large voltage hysteresis of the conversion reaction, prevent its practical use in lithium secondary batteries. In this study, the charge-discharge behavior of FeF_3 in an ionic liquid electrolyte at 363 K was investigated to elucidate the mechanisms and cause of the reduced overpotentials of the charge-discharge reactions. An evident plateau with an equilibrium potential of 3.42 V vs. Li^+/Li during the initial discharge, indicating the two-phase reaction of FeF_3 to form another phase nominally composed of non-trirutile-type $LiFe_2F_6$, was confirmed. Lithium cation was inserted into $LiFe_2F_6$, resulting in a gradual decrease in the rest potential. The lithium-inserted phase was finally converted to LiF and FeF_2 at the end of the one-electron discharge. The conversion of FeF_2 to LiF and Fe in the ionic liquid electrolyte at 363 K was completed at >2.0 V and 71.2 mA g^{-1}, even though the reaction did not occur at 298 K unless the electrode was discharged below 2.0 V. This difference in the operating voltage of the conversion reaction was mainly due to the suppression of the Li^+ diffusion overpotential at 363 K.

 [DOI: 10.1149/2.1151910jes]

Manuscript submitted April 9, 2019; revised manuscript received May 29, 2019. Published June 18, 2019.

Lithium secondary batteries have been utilized in electric vehicles, as well as portable devices, in recent years. Further utilization in the storage of surplus electricity is expected, and this requires a higher energy density and lower cost than those of current lithium secondary batteries.[1–6] In particular, the capacities of positive electrode materials require further improvement because they are generally insufficient compared with those of negative electrode materials, such as graphite, alloy-based materials, and lithium metal.[7–11] Metal fluorides are attractive candidates for positive electrode materials because in most cases, they have higher practical capacity based on both volume and weight, as well as higher reaction potential, than metal oxides. Particularly, iron trifluoride theoretically possesses a high capacity of 712 mAh g^{-1} and reasonably high average potential of 2.7 V vs. Li^+/Li for a three-electron reaction.[12–37]

The lithiation and delithiation of FeF_3 during the three-electron reaction occurs through insertion and conversion reactions. Several reaction mechanisms have been proposed for the first one-electron reaction, which depends on the starting material. Lithium insertion in nanosized FeF_3 to produce $LiFeF_3$ reportedly occurs through the formation of a solid solution.[29] Another study suggested the formation of $LiFe_2F_6$ based on the trirutile structure as an intermediate phase and further lithiation via a single-phase reaction.[20] On the other hand, another X-ray absorption study indicated that the conversion to LiF and FeF_2 occurs during the latter half of the one-electron reaction.[32] The following two-electron reaction was confirmed to be the conversion to LiF and Fe metal.[13]

Although untreated FeF_3 has a limited capacity of 80 mAh g^{-1} because of its low electronic conductivity,[12] a high capacity of 600 mAh g^{-1} was achieved by ball-milling with conductive carbon materials.[13] However, a solid-solid reaction between LiF and Fe during charging causes particle aggregation and consequently reduced cycleability.[36] This is exacerbated by the large voltage hysteresis between discharge and charge of more than 1 V, which leads to a serious loss of energy efficiency. Promotion of the charge reaction between LiF and Fe and addition of an anion receptor to the electrolyte solution to enhance the solubility of LiF improved the cycleability to an extent but did not suppress, however, the large voltage hysteresis.[35]

Theoretical, electrochemical, and spectroscopic analyses revealed that the conceivable causes of the large hysteresis are the different reaction paths between discharge and charge, overpotential of nucleation and growth during the conversion reaction, and diffusion overpotential of lithium in the solid phase.[32] A previous study employed galvanostatic intermittent titration technique (GITT) and potentiostatic intermittent titration technique (PITT) to separate the nucleation overpotential of the conversion reaction from the other overpotentials. It confirmed that the nucleation overpotential during discharge (about 0.2 V) is larger than that during charging and the diffusion coefficient of Li^+ in the solid state is very low ($\sim 10^{-18}$ cm^2 s^{-1}).[30]

In the present study, the charge-discharge behavior of FeF_3 in an ionic liquid at 363 K was investigated. Ionic liquids are suitable for this experimental condition, which requires high thermal stability of the electrolyte and solid electrolyte interface formed, owing to their unique properties, such as low volatility and low flammability. The Li[FSA]–[C_2C_1im][FSA] ($C_2C_1im^+$ = 1-ethyl-3-methylimidazolium, FSA^- = bis(fluorosulfonyl)amide) system was chosen as the electrolyte owing to its high ionic conductivity and sufficient electrochemical stability.[38–40] The intermediate-temperature operation of secondary batteries is of practical interest because of its effective use of waste heat.[41] In this instance, this operation was also expected to accelerate ion diffusion in the electrolyte and electrode and reduce the overpotential of the conversion reaction. The suppression of overpotentials enabled the observation of the (pseudo)equilibrium state, thereby giving insights on the charge-discharge mechanism. Herein, the reaction mechanism and effect of operation temperature on the overpotentials during discharge and charge were determined by X-ray diffraction (XRD) and GITT analyses.

Experimental

General procedures and electrode materials.—Materials were handled under dry argon atmosphere in a glove box. FeF_3 (reagent grade, Sigma-Aldrich) was dry-milled with acetylene black (AB; purity >99.99%, Wako Pure Chemical Industries) at a weight ratio of 70:25 using a planetary ball mill (Planetary Micro Mill PULVERISETTE 7 premium line, Fritsch) at 600 rpm for 8 h to form an FeF_3/AB composite. FeF_3/AB and polytetrafluoroethylene were well mixed at a weight ratio of 95:5 using an agate mortar and pestle until a homogeneous thin sheet was formed. The thin sheet was pressed onto an Al mesh and used as the FeF_3/AB positive electrode. Electrochemical measurements were performed using a two-electrode setup. The 2032 coin-type cells were assembled in an Ar-filled glove box using FeF_3 as the positive electrode, Li metal as the negative electrode, and a glass fiber filter separator (thickness = 260 μm, grade GF/A, Whatman). The 1 M $LiPF_6$/EC:DMC (EC = ethylenecarbonate and

*Electrochemical Society Member.
zE-mail: k-matsumoto@energy.kyoto-u.ac.jp

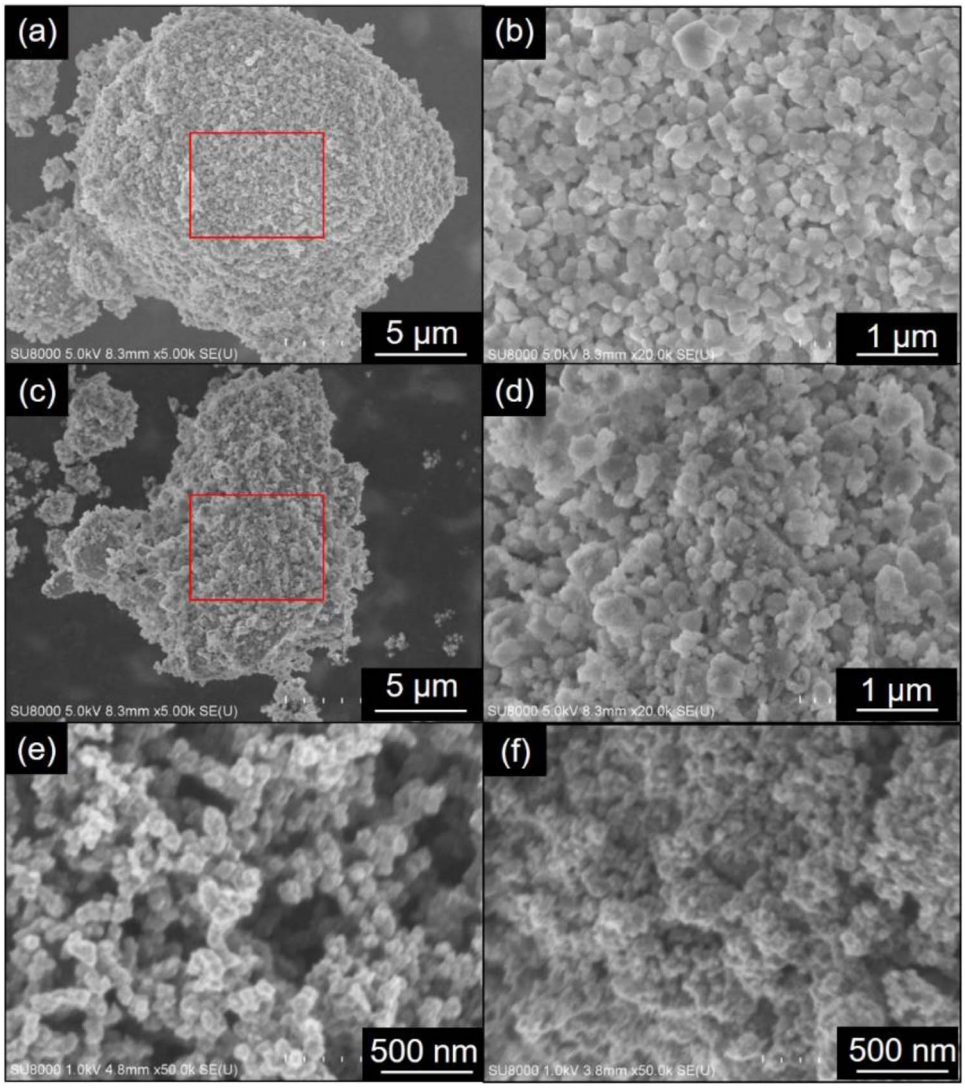

Figure 1. FE-SEM images of (a, b) pristine FeF_3, (c, d) FeF_3/AB composite after ball-milling, (e) pristine AB, and (f) AB after ball-milling. The red rectangles in (a) and (c) indicate the magnified regions shown in (b) and (d), respectively.

DMC = dimethylcarbonate; 1:1, v/v; lithium battery grade, Kishida Chemical) organic and Li[FSA]–[C_2C_1im][FSA] (3:7 mol/mol; Li[FSA], water content <20 ppm, Kishida Chemical and [C_2C_1im][FSA], water content <20 ppm, Kanto Chemical) ionic liquid electrolytes were used for the electrochemical measurements. Charge-discharge tests were conducted using the HJ-SD8 charge-discharge system (Hokuto Denko). To prepare the samples for XRD measurements, the coin-type cells were disassembled in the glove box after the charge-discharge test, and the FeF_3 electrodes were washed with tetrahydrofuran (water content <10 ppm, stabilizer free, Wako Pure Chemical Industries) and vacuum-dried at room temperature. All XRD samples were sealed in an air-tight cell with beryllium windows (Rigaku) filled with dry Ar to avoid exposure to air. XRD data were obtained using the SmartLab X-ray diffractometer (Rigaku) with Cu Kα radiation operated at 40 kV and 30 mA. The morphologies of the samples were observed by field-emission scanning electron microscopy (FE-SEM; SU8020, Hitachi). Overpotentials during charge and discharge were determined by GITT, which repeats the monitoring of voltage relaxation in the open circuit state immediately after charging or discharging to a certain state.

Results and Discussion

Morphology of FeF_3/AB composite.—Figure 1 shows the FE-SEM images of pristine FeF_3 and the FeF_3/AB composite obtained by ball-milling, as well as those of AB for comparison. Pristine FeF_3 consists of secondary particles around several tens of micrometer in diameter formed by the aggregation of primary particles around a few hundred nanometers in diameter (Figures 1a and 1b). These secondary particles are collapsed by ball-milling in the FeF_3/AB composite, whereas the size of the primary particles is scarcely changed (Figures 1c and 1d). In the FeF_3/AB composite (Figure 1d), the small particle of AB around FeF_3 (< 100 μm) is uniformly observed, although analysis by energy-dispersive X-ray spectroscopy at this resolution level is not possible at the current stage.

One-electron reaction of FeF_3/AB composite.—Figure 2 shows the discharge and charge curves of the FeF_3/AB electrode in 1 M $LiPF_6$/EC:DMC at 298 K and Li[FSA]–[C_2C_1im][FSA] at 363 K corresponding to the one-electron reaction. Although a comparison of discharge-charge data at 298 K reveals that there is a small polarization and large capacity in 1 M $LiPF_6$/EC:DMC (Figure 2a) compared with the case in Li[FSA]–[C_2C_1im][FSA] (Figure S1), the use of a higher operation temperature with the latter significantly improves the performance, which surpasses that in the organic electrolyte at 298 K. FeF_3 shows an initial discharge capacity of 201 mAh g^{-1} in Li[FSA]–[C_2C_1im][FSA] at 363 K, which is smaller than the theoretical capacity of 237 mAh g^{-1} for its one-electron reaction. The limited capacity may be due to its low crystallinity induced by ball-milling.

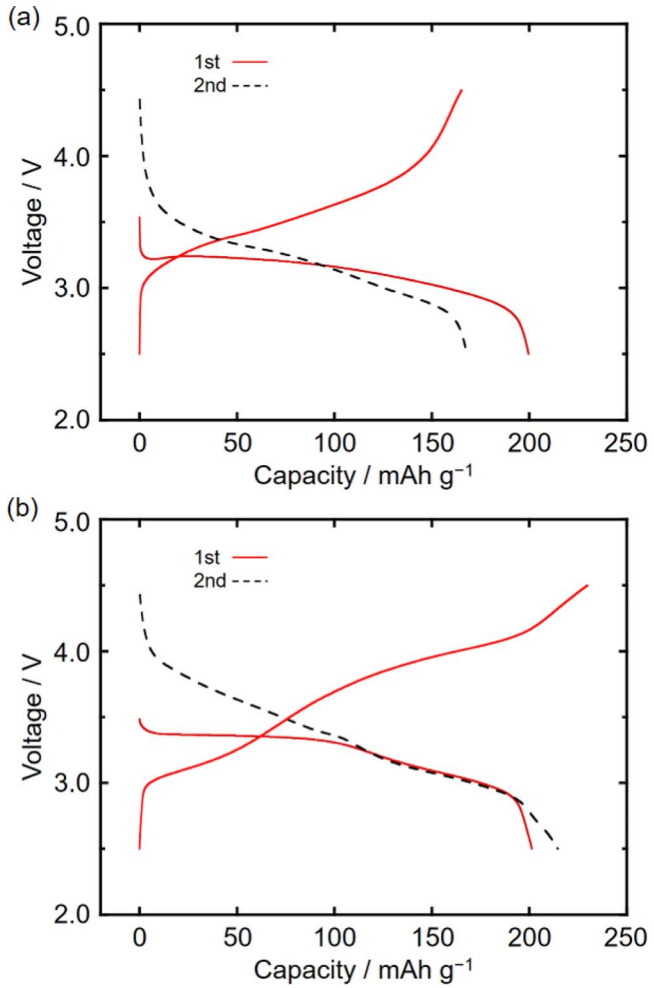

Figure 2. Discharge-charge curves of the FeF_3/AB electrode in (a) 1 M $LiPF_6$/EC:DMC at 298 K and (b) Li[FSA]–[C_2C_1im][FSA] at 363 K (current density: 100 mA g^{-1}, cutoff voltage: 4.5–2.5 V).

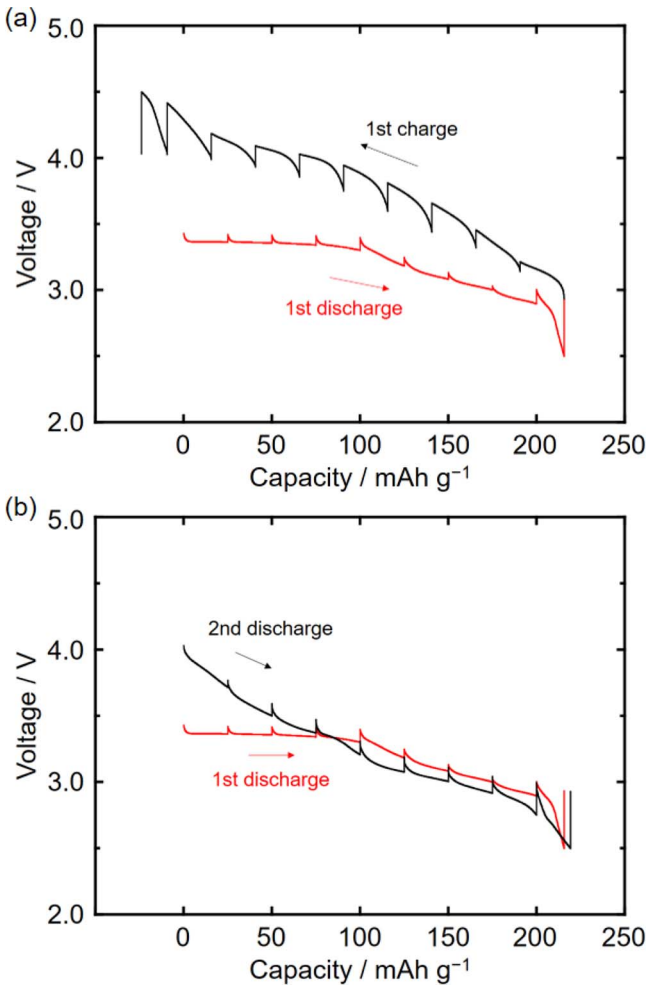

Figure 3. GITT curves during the (a) initial discharge-charge cycle and (b) initial and second discharge of the FeF_3/AB electrode in Li[FSA]–[C_2C_1im][FSA] at 363 K (polarization: 50 mA g^{-1} for 0.5 h, rest: 2.5 h, cutoff voltage: 4.5–2.5 V).

The following charge exhibits a capacity of 225 mAh g^{-1} with a gradual voltage increase to 4.5 V. In contrast to case in the organic electrolyte at 298 K, there is an evident plateau at 3.4 V during the initial discharge in the ionic liquid electrolyte at 363 K owing to enhanced Li^+ diffusion and electrode reaction. This indicates a two-phase reaction of FeF_3 to form another phase. The charge curve does not overlap with the initial discharge curve upon switching to charge in the middle of the plateau, indicating an irreversible reaction mechanism (Figure S2, Supporting Information). On the other hand, the second discharge shows no plateau even in the ionic liquid at 363 K, suggesting that the discharge reaction is different from that during the initial discharge.

Figure 3 shows the GITT curves of the FeF_3/AB composite in Li[FSA]–[C_2C_1im][FSA] at 363 K during the initial two cycles (see Figure S3, Supporting Information, for the time-voltage relationship). The curves were obtained under the conditions of charge or discharge at 50 mA g^{-1} for 0.5 h and subsequent rest for 2.5 h. The potential reaches a constant value of 3.42 V vs. Li^+/Li in the initial plateau region in Figure 3b. Regarding this plateau as a two-phase equilibrium between FeF_3 and $LiFe_2F_6$ (II) that does not have the trirutile structure (see the discussion of XRD results below), the standard Gibbs free energy of formation of $LiFe_2F_6$ (II), $\Delta_f G°(LiFe_2F_6$ (II)), at 363 K calculated from the equilibrium potential is -2.23×10^3 kJ mol^{-1} (see Supporting Information for details on the thermodynamic calculation). On the other hand, the $\Delta_f G°$ values of LiF, FeF_2, and FeF_3 are -5.80×10^2, -6.50×10^2, and -9.53×10^2 kJ mol^{-1}, respectively, at 363 K,[42] which sums to -2.18×10^3 kJ mol^{-1}. $\Delta_f G°(LiFe_2F_6$ (II)) is slightly smaller (i.e., more negative) than this value, indicating that $LiFe_2F_6$ (II) is more stable than the phase-separated state at 363 K.

The potential after relaxation gradually decreases to 2.95 V vs. Li^+/Li at the end of the plateau (1st discharge curve in Figure 3a), suggesting a single-phase reaction within this range. However, the overpotential increases and the relaxed potential decreases after the discharge capacity reaches around 200 mAh g^{-1}, suggesting that another reaction occurs at the end of the one-electron reaction.

In the subsequent first charge curve (1st charge curve in Figure 3a), the potential after relaxation monotonously increases with larger overpotentials than those during the first discharge. Moreover, the potential does not relax to the corresponding value during the first discharge. Although this may result from the slow relaxation after charging, the change in equilibrium potential is considered the main reason because complete amorphization is observed in the XRD pattern shown below. Although the potential after relaxation during the second discharge does not overlap with that during the first discharge and show a potential plateau in the initial stage, it gradually approaches that of the first discharge in the late stage (Figure 3b).

Figure 4 shows the ex situ XRD patterns of the FeF_3/AB electrode during the initial discharge and charge at 100 mA g^{-1}. The electrode at the plateau around 3.4 V during the initial discharge shows not the FeF_3 peaks, but two new peaks (marked with arrows in (B) in Figure 4) that were also observed in previous studies.[13,20] Although these two peaks were previously interpreted to be related to the 113 and 116

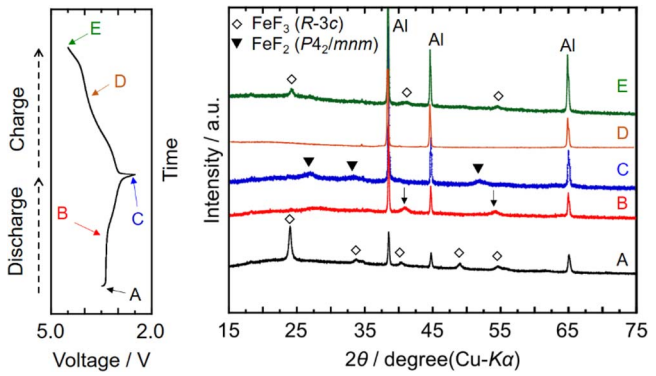

Figure 4. Ex situ XRD patterns of the FeF_3/AB electrode during the one-electron discharge-charge cycle at 363 K. The samples for ex-situ XRD were individually discharged (or charged) to the capacity corresponding to (A) to (E) in the discharge-charge curve on the left side. The peaks marked with arrows in pattern B are unknown.

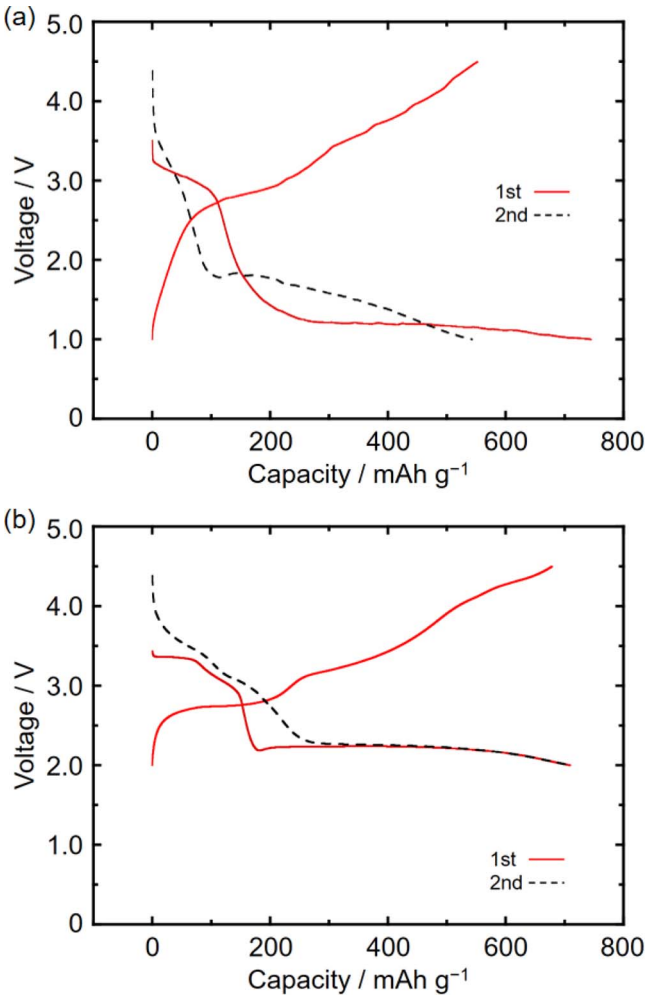

Figure 5. Discharge-charge curves of the FeF_3/AB electrode in (a) 1 M $LiPF_6$/EC:DMC at 298 K and (b) Li[FSA]–[C_2C_1im][FSA] at 363 K (current density: 71.2 mA g^{-1}, cutoff voltages: (a) 4.5–1.0 V and (b) 4.5–2.0 V).

diffraction lines of FeF_3 and a similar structural motif is locally preserved, the FeF_3 (*R*-3*c*) phase itself certainly disappears as all other diffraction peaks are absent. Further, these peaks do not agree with those of any of the previously proposed structures in the Li-Fe-F system, including trirutile-type $LiFe_2F_6$ ($P4_2/mnm$), rutile-type FeF_2 ($P4_2/mnm$) [or its derivatives, $LiFe_5F_{12}$ ($P4_2/mnm$), $LiFeF_4$ ($P2_1/c$), and Li_2FeF_6 ($P4_2/mnm$)], ilmenite-type Li_3FeF_6, or inverse spinel-type $Li_{15}Fe_3F_{24}$ ($P4_332$).[19] Nevertheless, the composition of this phase can be considered close to $LiFe_2F_6$ on the basis of the discharge capacity obtained in the present study. This interpretation agrees with the previously proposed one based on NMR data.[20] This phase is called $LiFe_2F_6$ (II) in this study, as already noted above, to distinguish it from trirutile-type $LiFe_2F_6$. The electrode discharged to 2.5 V shows weak peaks of FeF_2 (C). These XRD results support the discharge mechanism proposed by the GITT test involving lithium insertion into the new phase generated by the two-phase reaction and change in the crystal structure at the end of the one-electron discharge. Direct conversion from the $LiFe_2F_6$ (II) phase to LiF and FeF_2 was believed to occur in an organic electrolyte at room temperature.[32] In this study, which used an ionic liquid at 363 K, the combined results of GITT and XRD suggest the formation of a Li-rich, single-phase $LiFe_2F_6$ (II) via solid solution formation until the beginning of the conversion to LiF and FeF_2 at the end of the one-electron reaction (Figure 3b). Overall, the following three reactions occur stepwise during the initial discharge:

$$Li^+ + 2FeF_3 + e^- \rightarrow LiFe_2F_6\,(II)\,(\text{two-phase reaction}), \quad [1]$$

$$x\,Li^+ + LiFe_2F_6\,(II) + e^- \rightarrow Li_{1+x}Fe_2F_6(\text{single-phase reaction}), \quad [2]$$

$$(1-x)\,Li^+ + Li_{1+x}Fe_2F_6 + e^- \rightarrow LiF + FeF_2(\text{conversion reaction}). \quad [3]$$

The difference in mechanism from the previously proposed ones[13,20,43] is considered to arise from the different temperature, rate, and starting materials. During the following charge, the electrode charged to 4.0 V shows no peak (D), while the fully charged electrode shows weak peaks of FeF_3 (*R*-3*c*) (E). The crystallinity of the charged states decreases and is accompanied by structural change during the initial discharge.

Three-electron reaction of FeF_3/AB composite.—Figure 5 shows the initial discharge-charge and second discharge curves of the FeF_3/AB composite in 1 M $LiPF_6$/EC:DMC at 298 K and Li[FSA]–[C_2C_1im][FSA] at 363 K corresponding to the three-electron reaction. In the organic electrolyte at 298 K, the voltage suddenly drops after the one-electron reaction at ~3 V and ~150 mAh g^{-1}, and a long plateau is observed below 1.5 V, which is generally attributed to the conversion from FeF_2 or $LiFeF_3$ to LiF and Fe. Because this reaction requires a large overpotential at room temperature, it is not completed unless FeF_3 is discharged to about 1 V, resulting in a large voltage hysteresis between the discharge and charge curves. Although the overpotential in the second discharge is smaller than that in the initial discharge, the plateau potential is still lower than 2 V at 298 K. On the other hand, the initial discharge in the ionic liquid at 363 K shows a plateau at 3.4 V, followed by a gradual voltage decrease to 3 V, as observed in the one-electron reaction (Figure 2). The subsequent discharge exhibits a long plateau at around 2.2 V assignable to the conversion reaction, giving a discharge capacity of 711 mAh g^{-1}, which is close to the theoretical capacity for the three-electron reaction (712 mAh g^{-1}). Polarization in the region of the conversion reaction in the ionic liquid at 363 K is significantly suppressed compared with that in the organic electrolyte at 298 K. The plateau for this reaction is also observed at the same voltage during second discharge.

Figure 6 shows the discharge-charge curves of FeF_3 in Li[FSA]–[C_2C_1im][FSA] at 363 K during the initial 10 cycles. With each cycle, the discharge capacity gradually decreases with a coulombic efficiency above 97% and the voltage change becomes moderate throughout the capacity range. A previous theoretical study revealed that the reversibility of the reaction path is significantly influenced by the particle size of the original FeF_3 and current density. Moreover, it suggested the possibility of a complicated reaction path involving a series of Li–Fe–F ternary compounds.[19] Particle aggregation also reportedly

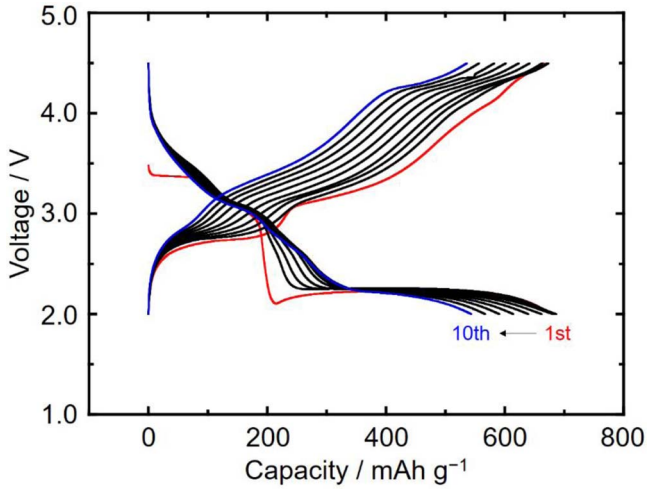

Figure 6. Discharge-charge curves of the FeF_3/AB electrode in Li[FSA]–[C_2C_1im][FSA] at 363 K during the initial 10 cycles (current density: 71.2 mA g^{-1}, cutoff voltage: 4.5–2.0 V).

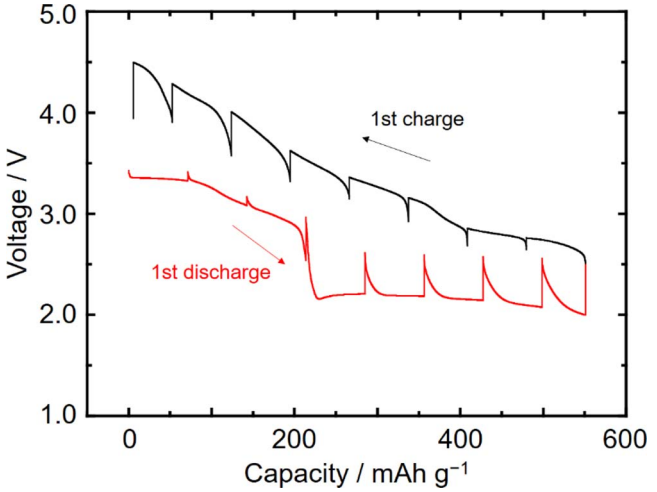

Figure 8. GITT curves during the initial discharge and charge of the FeF_3/AB electrode in Li[FSA]–[C_2C_1im][FSA] at 363 K (polarization: 71.2 mA g^{-1} for 1 h, rest: 5 h, cutoff voltage: 4.5–2.0 V).

occurs during the conversion reaction.[35] This, as well as the change in the reaction path during cycling, is likely promoted by the operation at 363 K.

The ex situ XRD patterns of the FeF_3/AB electrode during discharge and charge at 71.2 mA g^{-1} were measured to confirm that the conversion reaction proceeds during cycling, and the results are shown in Figure 7. The XRD pattern of the electrode at the plateau at 2.2 V (discharged for 5 h), which is ascribed to the conversion reaction, shows not the FeF_3 peaks, but the weak peaks assigned to FeF_2 and Fe (B). On the other hand, the electrode discharged to 2.0 V exhibits distinct Fe peaks (C). These results indicate that the conversion to LiF and Fe in the ionic liquid at 363 K is completed by discharging to 2.0 V, which suggests that the overpotential is reduced by ~1 V compared with that at 298 K. For the electrode sampled during the subsequent charge (charged for 5 h from 2.0 V), the diffraction peaks of Fe weaken and the FeF_2 peaks appear (D), which suggests that the reverse reaction from Fe and LiF to FeF_2 and Li^+ occurs. Overall, the plateau reaction at 2.2 V is the following conversion reaction:

$$2Li^+ + FeF_2 + 2e^- \rightarrow 2LiF + Fe(\text{conversion reaction}). \quad [4]$$

The electrode completely charged to 4.5 V shows no peaks (E), suggesting that it becomes amorphous owing to the poor growth of

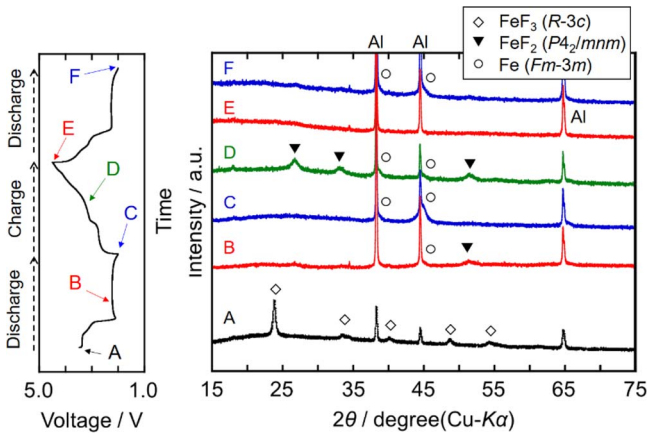

Figure 7. Ex situ XRD patterns of the FeF_3/AB composite electrode during the three-electron discharge-charge cycles at 363 K. The electrode states from (A) to (F) correspond to those in the discharge-charge curve on the left side.

the FeF_3 crystallites formed by the reverse conversion reaction of FeF_2 with residual LiF. The electrode re-discharged to 2.0 V shows the Fe peaks (F), suggesting that the conversion to LiF and Fe proceeds at the plateau around 2.2 V during the second discharge.

Figure 8 shows the GITT curve for the initial discharge-charge cycle in the ionic liquid at 363 K. Discharge at 71.2 mA g^{-1} for 1 h and open-circuit relaxation for 5 h were alternately repeated. The open-circuit potential at the plateau corresponding to the conversion reaction is approximately 2.55 V vs. Li^+/Li. The theoretical potential of the conversion to LiF and Fe (Eq. 4) at 363 K is 2.64 V vs. Li^+/Li (see Supporting Information for details on the thermodynamic calculation). The voltage is considered to relax almost completely at each open-circuit process by about 0.4–0.5 V, although the increment is 0.3 V or more at each initial short period (~1 h) (see Figure S4, Supporting Information, for the time-voltage relationship). In addition to the diffusion overpotentials, a short relaxation time for the nucleation and growth of Fe and LiF relative to that for diffusion is necessary during the conversion reaction. The present study suggests that nucleation and growth intrinsically require an overpotential of around 0.2–0.3 V even at 363 K. This value is similar to the nucleation overpotential (0.18 V) in ethyl methyl sulfone at 373 K observed in a previous study employing PITT.[30] In general, GITT tests indicate that FeF-based materials in an organic electrolyte at room temperature show a very slow and large voltage relaxation leading to a large voltage hysteresis over 1 V for the conversion reaction.[26] Because the reduction of nucleation and growth of particles is limited as shown above, the main difference in overpotential between 298 and 363 K is considered to result from the suppression of the diffusion overpotential. At the initial stage of the following charge, the potential relaxes to a value relatively close to that during discharge, suggesting the reversibility of the conversion reaction based on Eq. 4. However, the difference between the relaxation potentials gradually increases at higher states of charge, which indicates that the reaction heterogeneously proceeds from the surface to the core of the active material. In contrast to the case during discharge, the separated phases must be reversibly converted to a single phase through limited reaction paths. Such a heterogeneous reaction was indicated by a theoretical study, which proposed that the reaction paths of discharge and charge are different if the particle size of FeF_3 is above 10 nm because of slow Li^+ diffusion.[19] In the region above 3.0 V vs. Li^+/Li, the relaxation potential is similar to that for the one-electron reaction (Figure 3), suggesting that the same reaction occurs.

Reaction pathway of FeF_3 at 363 K.—Figure 9 summarizes the reaction pathway of the FeF_3/AB electrode during discharge at 363 K,

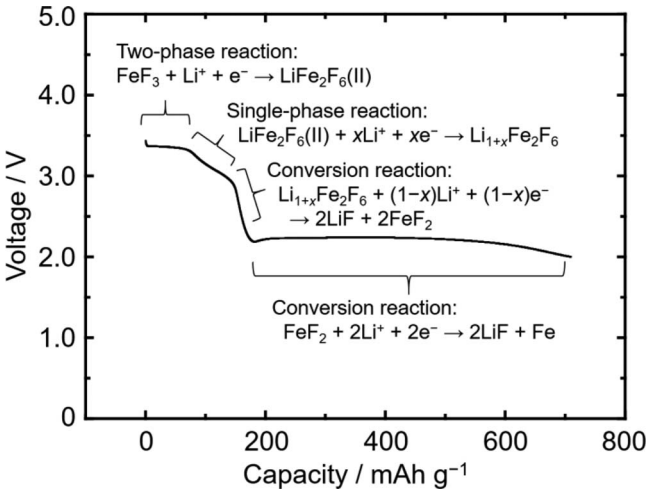

Figure 9. Summary of the reaction pathway of FeF_3 in Li[FSA]–[C_2C_1im][FSA] at 363 K during the initial discharge.

as clarified in this study. The one-electron reaction is exhibited as a distinct plateau at 3.4 V, which was not observed at 298 K and proceeded at a lower rate at 343 K.[13] Although this reaction is irreversible, it corresponds to the two-phase reaction of FeF_3 to form another phase nominally composed of $LiFe_2F_6$ that does not have the trirutile structure [$LiFe_2F_6$ (II)] (Eq. 1). Further discharge leads to the formation of the $Li_{1+x}Fe_2F_6$ solid solution phase (Eq. 2) and finally to the conversion to LiF and FeF_2 (Eq. 3) even during the one-electron reaction. For the three-electron reaction, a significant reduction in overpotential (∼1 V) is especially observed for the conversion to LiF and Fe (Eq. 4) owing to enhanced kinetics caused by temperature elevation. The reverse conversion from LiF and Fe occurs in the same path at the beginning of the charging step and proceeds slowly, reaching the formation of FeF_2 by two-electron oxidation. The last one-electron reaction during charging appears to be similar to the case without the conversion reaction (Eq. 4) and reaches the amorphous product at the end. This is in contrast to the formation of crystalline FeF_3 (*R*-3*c*) when the electrode is immediately oxidized after one-electron reduction.

Conclusions

This study investigated the charge-discharge behavior of FeF_3 in the Li[FSA]–[C_2C_1im][FSA] ionic liquid at 363 K by galvanostatic charge-discharge, XRD, and GITT measurements. Elevation of the operation temperature clearly showed the differences in the charge-discharge behavior and reduction of overpotentials especially for the conversion reaction. The formation of a phase nominally composed of $LiFe_2F_6$ without the trirutile structure during discharge via the two-phase reaction of FeF_3 was certainly confirmed. The conversion to FeF_2 during one-electron reduction, which was controversial in previous works, was confirmed to occur at the end of the process. The discharge voltage exceeding 2 V for the three-electron reaction also implies the possible operation of the FeF_3 positive electrode at 363 K. Although the cycling properties require further improvement even at 363 K, the present study showed that elevation of the operation temperature is an effective way of overcoming the large overpotentials and slow reaction kinetics of metal fluorides in practical applications.

Acknowledgments

This work was partly supported by the Research Fellowship Program for Young Scientists, the Japan Society for the Promotion of Science (17J09968).

ORCID

Kazuhiko Matsumoto https://orcid.org/0000-0002-0770-9210
Rika Hagiwara https://orcid.org/0000-0002-7234-3980

References

1. J. B. Goodenough and Y. Kim, *Chem. Mater.*, **22**, 587 (2010).
2. V. Etacheri, R. Marom, R. Elazari, G. Salitra, and D. Aurbach, *Energy Enviro. Sci.*, **4**, 3243 (2011).
3. J. B. Goodenough and K.-S. Park, *J. Am. Chem. Soc.*, **135**, 1167 (2013).
4. B. Scrosati, J. Hassoun, and Y.-K. Sun, *Energ. Environ. Sci.*, **4**, 3287 (2011).
5. B. Dunn, H. Kamath, and J.-M. Tarascon, *Science*, **334**, 928 (2011).
6. Z. Yang, J. Zhang, M. C. Kintner-Meyer, X. Lu, D. Choi, J. P. Lemmon, and J. Liu, *Chem. Rev.*, **111**, 3577 (2011).
7. M. S. Whittingham, *Chem. Rev.*, **104**, 4271 (2004).
8. M. V. Reddy, G. V. S. Rao, and B. V. R. Chowdari, *Chem. Rev.*, **113**, 5364 (2013).
9. A. F. Gonzalez, N.-H. Yang, and R.-S. Liu, *J. Phys. Chem. C*, **121**, 27775 (2017).
10. S.-H. Yu, S. H. Lee, D. J. Lee, Y.-E. Sung, and T. Hyeon, *Small*, **12**, 2146 (2016).
11. K. Chen and D. Xue, *J. Mater. Chem. A*, **4**, 7522 (2016).
12. H. Arai, S. Okada, Y. Sakurai, and J. Yamaki, *J. Power Sources*, **68**, 716 (1997).
13. F. Badway, F. Cosandey, N. Pereira, and G. G. Amatucci, *J. Electrochem. Soc.*, **150**, A1318 (2003).
14. H. Li, G. Richter, and J. Maier, *Advanced Materials*, **15**, 736 (2003).
15. H. Li, P. Balaya, and J. Maier, *J. Electrochem. Soc.*, **151**, A1878 (2004).
16. I. Plitz, F. Badway, J. Al-Sharab, A. DuPasquier, F. Cosandey, and G. G. Amatucci, *J. Electrochem. Soc.*, **152**, A307 (2005).
17. M. Nishijima, I. D. Gocheva, S. Okada, T. Doi, J. Yamaki, and T. Nishida, *J. Power Sources*, **190**, 558 (2009).
18. G. G. Amatucci and N. Pereira, *J. Fluorine Chem.*, **128**, 243 (2007).
19. R. E. Doe, K. A. Persson, Y. S. Meng, and G. Ceder, *Chem. Mater.*, **20**, 5274 (2008).
20. N. Yamakawa, M. Jiang, B. Key, and C. P. Grey, *J. Am. Chem. Soc.*, **131**, 10525 (2009).
21. T. Li, L. Li, Y. L. Cao, X. P. Ai, and H. X. Yang, *J. Phys. Chem. C*, **114**, 3190 (2010).
22. S.-W. Kim, D.-H. Seo, H. Gwon, J. Kim, and K. Kang, *Adv. Mater.*, **22**, 5260 (2010).
23. M. Zhou, L. Zhao, T. Doi, S. Okada, and J. Yamaki, *J. Power Sources*, **195**, 4952 (2010).
24. N. Yabuuchi, M. Sugano, Y. Yamakawa, I. Nakai, K. Sakamoto, H. Muramatsu, and S. Komaba, *J. Mater. Chem.*, **21**, 10035 (2011).
25. M. Zhou, L. Zhao, A. Kitajou, S. Okada, and J. Yamaki, *J. Power Sources*, **203**, 103 (2012).
26. P. Liu, J. J. Vajo, J. S. Wang, W. Li, and J. Liu, *J. Phys. Chem. C*, **116**, 6467 (2012).
27. C. Li, X. Mu, P. A. van Aken, and J. A. Maier, *Adv. Energy Mater.*, **3**, 113 (2013).
28. J. Liu, Y. Wan, W. Liu, Z. Ma, S. Ji, J. Wang, Y. Zhou, P. Hodgson, and Y. Li, *J. Mater. Chem. A*, **1**, 1969 (2013).
29. H. J. Tan, H. L. Smith, L. Kim, T. K. Harding, S. C. Jones, and B. Fultz, *J. Electrochem. Soc.*, **161**, A445 (2014).
30. J. K. Ko, K. M. Wiaderek, N. Pereira, T. L. Kinnibrugh, J. R. Kim, P. J. Chupas, K. W. Chapman, and G. G. Amatucci, *Acs Appl. Mater. Inter.*, **6**, 10858 (2014).
31. M. Zhou, L. Zhao, S. Okada, and J. Yamaki, *J Power Sources*, **253**, 74 (2014).
32. L. Li, R. Jacobs, P. Gao, L. Gan, F. Wang, D. Morgan, and S. Jin, *J. Am. Chem. Soc.*, **138**, 2838 (2016).
33. D. Dambournet, M. Duttine, K. W. Chapman, A. Wattiaux, O. Borkiewicz, P. J. Chupas, A. Demourgues, and H. Groult, *J. Phys. Chem. C*, **118**, 14039 (2014).
34. M. Burbano, M. Duttine, O. Borkiewicz, A. Wattiaux, A. Demourgues, M. Salanne, H. Groult, and D. Dambournet, *Inorg. Chem.*, **54**, 9619 (2015).
35. K. Kumagae, K. Okazaki, K. Matsui, H. Horino, T. Hirai, J. Yamaki, and Z. Ogumi, *J. Electrochem. Soc.*, **163**, A1633 (2017).
36. T. Takami, K. Matsui, H. Senoh, N. Taguchi, M. Shikano, H. Sakaebe, and T. J. Fukunaga, *J. Alloys Compounds*, **769**, 539 (2018).
37. S. Tawa, Y. Sato, Y. Orikasa, K. Matsumoto, and R. Hagiwara, *J. Power Sources*, **412**, 180 (2019).
38. H. Zhang, W. Feng, J. Nie, and Z. Zhou, *J. Fluorine Chem.*, **174**, 49 (2015).
39. H. Matsumoto, H. Sakaebe, K. Tatsumi, M. Kikuta, E. Ishiko, and M. Kono, *J. Power Sources*, **160**, 1308 (2006).
40. K. Matsumoto, E. Nishiwaki T. Hosokawa, S. Tawa, T. Nohira, and R. Hagiwara, *J. Phys. Chem. C*, **121**, 9209 (2017).
41. J. Hwang, K. Matsumoto, and R. Hagiwara, *Adv. Sustainable Syst.*, **2**, 1700171 (2018).
42. M. W. Chase Jr., *NIST-JANAF Themochemical Tables, Fourth Edition, J. Phys. Chem. Ref. Data, Monograph*, **9**, (1998).
43. A. Kitajou, I. Tanaka, Y. Tanaka, E. Kobayashi, H. Setoyama, T. Okajima, and S. Okada, *Electrochemistry*, **85**, 427 (2017).